Optimal allocation of Renewable Energy Systems in a Weak Distribution Network

Markus Miller*, José Luis Paternina†§, Sergio F. Contreras*, Camilo A. Cortes† and Johanna M.A. Myrzik*
* Institute of Automation Technology - IAT
University of Bremen, Bremen, Germany
miller@iat.uni-bremen.de
† Department of Electrical and Electronic Engineering
Universidad Nacional de Colombia, Bogotá, Colombia
jpaterninad@unal.edu.co
§Faculty of Electronic Engineering
Universidad Santo Tomás, Bogotá, Colombia
jose.paternina@usta.edu.co

***Abstract*—In the context of a real electrical distribution network in Puerto Carreño, Colombia, this paper addresses the challenge of enhancing power supply reliability through the strategic integration of Renewable Energy Sources with Hydrogen Energy Systems. The planning problem is reformulated as a Mixed-Integer Quadratically Constrained Programming problem, enabling the use of efficient solvers with global optimal solution. Considering the extensive curtailment options and numerous allocation components, the optimization problem naturally scales up. To address this computational intensity, representative scenarios are derived from the original high-dimensional probability distribution employing the Gaussian Mixture Model. These scenarios are used in conjunction with the proposed optimization framework to achieve cost-effective power grids while reducing fossil fuel dependency.**

***Index Terms*—Hydrogen energy systems, Renewable energy systems, Optimal allocation, Distribution networks, Reliability enhancement**

I. Introduction

Distribution networks stand as the backbone of electrical systems, holding a substantial share in power system investments. This significance has spurred extensive research on planning problems in distribution systems, aiming to enhance various aspects such as providing ancillary services like residual power to the main grid [1], reactive power control due to inverters [2], and developing planning frameworks that consider both short and long terms [3]. Recent studies have primarily concentrated on optimizing the location and sizing of Distributed Energy Resources (DERs), including Renewable Energy Sources (RESs) and Battery Energy Storage Systems (BESSs) for grid [4] or island mode [5]. Amid the growing focus on decarbonization goals [6], the integration of RESs is paramount. Despite their potential, the existing BESSs grapple with limitations in energy storage capacity, proving them suitable for short-duration cycles but not for prolonged power supply interruptions [7]. This limitation underscores the necessity to explore new storage mechanisms [8].

In the field of power systems, especially those with significant integration of RESs, addressing uncertainties is a common challenge [9]. These uncertainties, arising from unpredictable weather patterns [10], increasing load growth [11], and contingencies of power system components, have been traditionally tackled using stochastic programming. This method, widely used in the operation and planning of power grids [12], often requires a large number of samples for the optimization framework, leading to a substantial computational burden. Additionally, managing non-linear equations coupled with a multitude of integer variables significantly increases the computational burden.

Moreover, the concept of a weak distribution network, illustrated by Puerto Carreño's power grid, introduces additional complexity. These networks face challenges with insufficient generator capacities to meet peak demands, especially during contingencies. Puerto Carreño's situation is particularly challenging due to its reliance on an unstable connection to the external grid, which is its link to neighboring Venezuela, rather than a direct connection to Colombia's transmission grid. The endeavor to enhance the power system's robustness and reliability significantly adds to the computational burden, especially when considering numerous potential scenarios and contingencies.

Meta-heuristic techniques, which are state-of-the-art in navigating these complexities, offer an advantage with their ease of implementation. For instance, recent studies, such as one introduced by [13], have showcased a microgrid planning model that integrates wind turbines, photovoltaics (PV), fuel cells, and combined heat and power units. This model, aimed at ensuring the microgrid's generation meets both electrical and thermal demands, is optimized using an enhanced particle swarm optimization algorithm. Despite the adaptability of meta-heuristic methods, their limitations in guaranteeing globally optimal solutions become more evident as the scale of the problem increases.

However, our novel application of Mixed-Integer Quadratically Constrained Programming (MIQCP) with an innovative scenario generation technique effectively addresses this challenge. Our approach not only offers a cost-effective solution

but also increases the system's robustness, making it particularly suitable for situations like that in Puerto Carreño.

To demonstrate the methodology's effectiveness, PVs, electrolyzers, and fuel cells are optimally allocated in a weak distribution grid, defined by its intermittent external connection and lack of adequate backup generation capacity during contingencies. The objective is to strengthen the grid's robustness, minimize costs, and achieve decarbonization goals. The main contributions are:

1) A new planning methodology for the integration of photovoltaics coupled with electrolyzers and fuel cells to improve technical and economical aspects of a weak distribution grid.
2) A novel approach for representing a high-dimensional probability distribution with highly representative scenarios.
3) Validation of the methodologies on a real distribution network in Puerto Carreño, Colombia (see Fig. 1).

The organization of this paper is as follows: Section II introduces the scenario generation methodology. Section III covers PV and hydrogen component modeling. The mathematical formulation of the optimization problem is presented in Section IV, followed by insights from a case study in Puerto Carreño, Colombia in Section V. Section VI showcases the results, leading to the conclusion in Section VII. For a comprehensive overview of the variables and constants, readers are directed to Appendix A.

II. Representative scenario generation

In this study, timeseries data are given for active power load $\mathrm{P}^{\mathrm{L}}_{jt}$ and reactive power load $\mathrm{Q}^{\mathrm{L}}_{jt}$ at node j, ambient air temperature T_t, and solar irradiance G_t, at time point t. With this data set a high-dimensional probability distribution, $\mathrm{p}(\mathrm{P}^{\mathrm{L}}_j, \mathrm{Q}^{\mathrm{L}}_j, \mathrm{T}, \mathrm{G})$ is generated. Monte Carlo Sampling, a traditional method for drawing random samples from a probability distribution, is commonly used in stochastic programming within optimization frameworks. Despite its widespread use, this method frequently faces the challenge of high variance in the sampled data. Solving this issue requires a substantial amount of random samples to achieve an accurate representation of the original high-dimensional probability distribution, resulting in significant computational overhead for optimization tasks.

This work adopts the Gaussian Mixture Model (GMM) as an alternative for estimating probability distributions. This technique utilizes multivariate Gaussian distributions, each defined by a mean μ_s and a covariance matrix $\mathbf{\Sigma}_s$, to approximate the original distribution. A detail explanation is available in [14]. Unlike robust optimization, which tends toward conservative outcomes by focusing on worst-case scenarios, GMM enables a balanced exploration of possible outcomes, enhancing both the precision and computational efficiency of the planning methodology. The mean value μ_s from each cluster s is decomposed into the original variables $\mathrm{P}^{\mathrm{L}}_{js}$, $\mathrm{Q}^{\mathrm{L}}_{js}$, T_s and G_s, forming a representative scenario with a corresponding likelihood based on the number of scenarios the Gaussian distribution represents. The choice of GMM over K-means clustering [15] is motivated by its adeptness in fitting ellipsoidal distributions, a critical characteristic for managing correlated variables. In summary, the GMM approach estimates the original high-dimensional probability distribution using significantly fewer scenarios, ensuring both computational efficiency and representational accuracy.

Unforeseen events, like power system component outages, have a substantial impact on the performance and reliability of a power system. Such contingency scenarios are represented by the index w. This notation is used in Section IV to indicate and manage the components experiencing an outage, by setting their operating ranges to zero.

III. Models

A. RES production (PV generators)

At a specific scenario s, the PV production is influenced by various factors such as solar irradiance G_s, ambient air temperature T_s, and the type of PV cell model [16]. The PV cell temperature T_{PV} is determined by (1). The nominal operating cell temperature (NOCT) is provided by the manufacturer and is set to $45^{\mathrm{o}}\mathrm{C}$ in this study.

$$\mathrm{T}_{\mathrm{PV}} = \mathrm{T}_s + \frac{\mathrm{NOCT} - 20^{\mathrm{o}}\mathrm{C}}{800\frac{\mathrm{W}}{\mathrm{m}^2}} \cdot \mathrm{G}_s \tag{1}$$

The temperature correction factor, denoted as γ_{Ts}, is determined in (2). It depends on the the power variation coefficient $\mathrm{p}_{\mathrm{coef}}$ and the PV cell cell temperature T_{PV}. In this study, $\mathrm{p}_{\mathrm{coef}}$ is assigned a value of $-3.5 \cdot 10^{-3} (1/^{\circ}\mathrm{C})$ [17]. This coefficient causes the term $\mathrm{p}_{\mathrm{coef}} \cdot (\mathrm{T}_{\mathrm{PV}} - 25^{\mathrm{o}}\mathrm{C})$ to be negative when the cell temperature exceeds the reference cell temperature of $25^{\mathrm{o}}\mathrm{C}$, leading to a reduction in γ_{Ts}.

$$\gamma_{Ts} = (1 + \mathrm{p}_{\mathrm{coef}} \cdot (\mathrm{T}_{\mathrm{PV}} - 25^{\mathrm{o}}\mathrm{C})) \tag{2}$$

Under standard test condition, the solar irradiance correction factor, denoted as λ_{Gs}, is determined using a linear relationship as illustrated in (3) and referenced in [18].

$$\lambda_{Gs} = \frac{\mathrm{G}_s}{1000\frac{\mathrm{W}}{\mathrm{m}^2}} \tag{3}$$

For solar irradiance values G_s exceeding $1000\,\mathrm{W/m^2}$, λ_{Gs} is capped at 1. The overall efficiency η^{PV}_s is a product of the temperature correction factor, solar irradiance correction factor and the inverter efficiency $\eta^{\mathrm{PV}}_{\mathrm{conv}}$, as shown in (4).

$$\epsilon^{\mathrm{PV}}_s = \gamma_{Ts} \cdot \lambda_{Gs} \cdot \eta^{\mathrm{PV}}_{\mathrm{conv}} \tag{4}$$

The rated power of a PV is then used in conjunction with the effective power coefficient of the PV, denoted as ϵ^{PV}_s, to determine the true power output for a scenario s. Detailed values and coefficients used in the PV model are provided in Section VI under Table (IV).

B. Power - To - X Technology - PEM Electrolyzer

Several electrolyzer technologies are currently available. However, according to various authors [18], [19], the Proton Exchange Membrane (PEM) Electrolyzer stands out as the most developed and suitable for power system applications because of the general higher efficiency and the faster response time. It is important to have a fast response time because of the dynamic load behaviour and the random power generation from RESs. Consequently, the model presented in (5) focuses on this specific technology.

$$\mathrm{H}^{+}_{2,jsw} = \frac{\eta_{\mathrm{EL}}}{\zeta_{\mathrm{H_2}}} \cdot \mathrm{P}^{\mathrm{EL}}_{j,sw} = \alpha_{\mathrm{EL}} \cdot \mathrm{P}^{\mathrm{EL}}_{j,sw} \tag{5}$$

$\mathrm{H}^{+}_{2,jsw}$ denotes the hydrogen production at a specific node j, for a given scenario s, and under a particular contingency w, measured in kilograms (kg). η_{EL} represents the efficiency of the electrolyzer. $\mathrm{P}^{\mathrm{EL}}_{j,sw}$ is the power input to the electrolyzer. The time interval is set to 1 hour for this study. $\zeta_{\mathrm{H_2}}$ is the higher heating value of hydrogen [18].

C. Fuel Cell

The Fuel Cell (FC) is an assembly of individual fuel cells stacked to a single unit with a higher maximum power output. For a seamless system integration, the FC in this study will also adopt the PEM technology. To produce power from the FC, hydrogen has to be consumed based on (6).

$$\mathrm{H}^{-}_{2,jsw} = \left(\alpha_{\mathrm{FC}} \cdot \mathrm{P}^{\mathrm{FC}}_{j} + \beta_{\mathrm{FC}} \cdot \mathrm{p}^{\mathrm{FC}}_{jsw}\right) \cdot \mathrm{x}^{\mathrm{FC}}_{jsw} \tag{6}$$

$\mathrm{P}^{\mathrm{FC}}_{j}$ is the FC capacity. The consumption coefficients, α_{FC} and β_{FC} are derived from the fuel cell's hydrogen consumption curve [19]. The variable $\mathrm{p}^{\mathrm{FC}}_{jsw}$ corresponds to the FC output power for a node j, scenario s and contingency w. $\mathrm{x}^{\mathrm{FC}}_{jsw}$ denotes the operational state of the FC, with a value of 1 indicating an active state and 0 a deactive state. The hydrogen consumption, comprises of two components. The first is a constant value determined by the size of $\mathrm{P}^{\mathrm{FC}}_{j}$, the second component increases linearly depending on the required power output $\mathrm{p}^{\mathrm{FC}}_{jsw}$.

IV. Optimal Allocation of Hydrogen Components and PV Systems

1) Extended Relaxation of Power Flow: Traditionally, power flow equations are nonlinear. However, by employing the methodology presented in [20], these equations can be transformed into a Second Order Cone Programming (SOCP) framework. This is achieved by squaring the original branch flow equations, thereby converting the problem into a convex optimization format.

Given a current I_{ijsw} flowing through a conductor ij and a voltage V_{j} at node j, these variables are squared to derive the new variables l_{ijws} and v_{jsw}, as depicted in (7).

$$\mathrm{l}_{ijsw} = |\mathrm{I}_{ijsw}|^2 \tag{7a}$$
$$\mathrm{v}_{jsw} = |\mathrm{V}_{jsw}|^2 \tag{7b}$$

The relaxed branch flow equations are derived from [20] and presented in equations (8)–(11).

$$\begin{aligned}\mathrm{p}^{\mathrm{G}}_{jsw} + \mathrm{p}^{\mathrm{FC}}_{jsw} = \mathrm{P}^{\mathrm{L}}_{js}\mathrm{x}^{\mathrm{L}}_{jsw} + \mathrm{p}^{\mathrm{EL}}_{jsw} + \sum_{i\in \mathrm{N}_{\mathrm{from}}(j)} \mathrm{P}_{jisw} \\ - \sum_{i\in \mathrm{N}_{\mathrm{to}}(j)} (\mathrm{P}_{ijsw} - \mathrm{r}_{ij}\mathrm{l}_{ijsw})\end{aligned} \tag{8}$$

$$\begin{aligned}\mathrm{q}^{\mathrm{G}}_{jsw} = \mathrm{Q}^{\mathrm{L}}_{js}\mathrm{x}^{\mathrm{L}}_{jsw} + \sum_{i\in \mathrm{N}_{\mathrm{from}}(j)} \mathrm{Q}_{jisw} \\ - \sum_{i\in \mathrm{N}_{\mathrm{to}}(j)} (\mathrm{Q}_{ijsw} - \mathrm{x}_{ij}\mathrm{l}_{ijsw})\end{aligned} \tag{9}$$

$$\mathrm{v}_{jsw} = \mathrm{v}_{isw} - 2(\mathrm{r}_{ij}\mathrm{P}_{ijsw} + \mathrm{x}_{ij}\mathrm{Q}_{ijsw}) + (\mathrm{r}^2_{ij} + \mathrm{x}^2_{ij})\mathrm{l}_{ijsw} \tag{10}$$

$$\mathrm{l}_{ijsw}\mathrm{v}_{isw} \geq \mathrm{P}^2_{ijsw} + \mathrm{Q}^2_{ijsw} \tag{11}$$

The power balancing equations, (8) and (9), have been expanded to incorporate the power generation from the fuel cell $\mathrm{p}^{\mathrm{FC}}_{js}$, power consumption of the electrolyzer $\mathrm{p}^{\mathrm{EL}}_{js}$, the true active and reactive power generation of the PV $\mathrm{p}^{\mathrm{G}}_{jsw}$ and $\mathrm{q}^{\mathrm{G}}_{jsw}$ and the curtailment possibility $\mathrm{x}^{\mathrm{L}}_{jsw}$ for the active and reactive load. The equations (8), (9) are defined for all $j \in \mathrm{N}$ and equations (10), (11) are defined for all $i, j \in \mathrm{E}$. $\mathrm{p}^{\mathrm{G}}_{jsw} = \mathrm{x}^{\mathrm{G}}_{jsw}\mathrm{x}^{\mathrm{G}}_{j}\mathrm{P}^{\mathrm{G}}_{j}\epsilon^{\mathrm{PV}}_{s}$, which combines curtailment $\mathrm{x}^{\mathrm{G}}_{jsw}$, placement decision $\mathrm{x}^{\mathrm{G}}_{j}$, capacity $\mathrm{P}^{\mathrm{G}}_{j}$ and the effective power coefficient $\epsilon^{\mathrm{PV}}_{s}$ of the PV, defined in III-A. The reactive power has a similar definition with $\mathrm{q}^{\mathrm{G}}_{jsw} = \mathrm{x}^{\mathrm{G}}_{jsw}\mathrm{x}^{\mathrm{G}}_{j}\mathrm{Q}^{\mathrm{G}}_{jsw}$.

To make the best use of quadratic programming solvers, these cubic terms are transformed into quadratic terms. Specifically the product of the generator placement variable $\mathrm{x}^{\mathrm{G}}_{j}$ and the generator curtailment $\mathrm{x}^{\mathrm{G}}_{jsw}$ is substituted by the new variable $\mathrm{w}^{\mathrm{G}}_{jsw}$, as detailed in [21]. The new relationships are shown in equation (12), with additional constraints provided in equations (13)–(15) to ensure valid representation.

$$\mathrm{p}^{\mathrm{G}}_{js} = \mathrm{w}^{\mathrm{G}}_{jsw}\mathrm{P}^{\mathrm{G}}_{j}\epsilon^{\mathrm{PV}}_{s} \tag{12a}$$
$$\mathrm{q}^{\mathrm{G}}_{js} = \mathrm{w}^{\mathrm{G}}_{jsw}\mathrm{Q}^{\mathrm{G}}_{jsw} \tag{12b}$$

$$\mathrm{w}^{\mathrm{G}}_{js} \leq \mathrm{x}^{\mathrm{G}}_{js} \tag{13}$$
$$\mathrm{w}^{\mathrm{G}}_{js} \leq \mathrm{x}^{\mathrm{G}}_{j} \tag{14}$$
$$\mathrm{x}^{\mathrm{G}}_{js} + \mathrm{x}_{j} - 1 \leq \mathrm{w}^{\mathrm{G}}_{js} \tag{15}$$

Equations (8) through (15) comprehensively describe the extended power flow equations.

2) Mixed Integer Quadratically Constrained Programming Model for Optimal Allocation of Hydrogen and PV Components: The objective of the MIQCP problem for optimal allocation of hydrogen and PV systems is to minimize the total present value cost of the power system, as depicted in (16). This total cost encompasses the investment cost (17), the present value of operation and maintenance (O&M) cost (18), and a scenario-contingency cost C_{sw} (19), which is weighted by its probability of occurrence p_{sw}. Including present value cost is vital, as it translates future costs to current values, aiding in the precise economic assessment of power system

investments over the project's lifespan. The discount rate is set to $\mathrm{r} = 3\%$, and the lifespan of all devices is determined to be $\mathrm{N_{years}} = 20$. The detailed breakdown of C_{sw} is provided from (20)–(22), which includes costs associated with external grid utilization, diesel fuel consumption, and load curtailment cost. As shown in equation (20), the distribution grid can either consume power from the external grid or feed power back into it at a reduced rate. To ensure the operational logic of grid interaction is accurately represented, two additional constraints, designated as equations (23a) and (23b), are introduced. Alongside the binary variable b_{sw}, which indicates the direction of power flow, these constraints incorporate $\mathrm{P^{EG}}$, the maximum power capacity for transactions with the external grid. This approach is commonly known in operations research as the big M method.

Equation (16) is minimized subject to the extended power flow equations (8)–(15) and the constraints (23a)–(34). (25)–(28) are defined for all nodes. These constraints include current limits through lines (24) and voltage limits (25). Equations (26) and (27) detail the hydrogen production and consumption dynamics of the electrolyzer and fuel cell, respectively. Although our probabilistic approach eliminates the temporal correlations, it is not directly suitable for optimizing the size of the hydrogen tanks due to their time-dependent state. While the tank size can be determined post hoc, it is not the primary focus of this study. To ensure a balance between hydrogen production and consumption, (28) is incorporated. Component size constraints are outlined in (29). Notably, $\mathrm{P}^{\mathrm{G}}_{j}$ has a lower bound $\mathrm{P}^{\mathrm{G}}_{\min}$ to prevent the allocation of inordinately small PVs. Such PVs might be used solely for leveraging the inverter to control node voltage, thereby influencing the reactive power flow $\mathrm{Q}^{\mathrm{G}}_{jsw}$. Operational constraints for the fuel cell and electrolyzer are provided in (30). Similarly, operational limits for the external grid and diesel generators are detailed in (31), with the matrix (35) dictating the activation or deactivation of generator functionalities in response to contingencies.

$$\min \left(\mathrm{C_{inv}} + \mathrm{C_{OM}} + \sum_{t=1}^{\mathrm{N_{years}}} \frac{\mathrm{N_{span}}}{(1+\mathrm{r})^t} \cdot \sum_{w \in W} \sum_{s \in S} p_{sw} \mathrm{C}_{sw} \right) \tag{16}$$

$$\mathrm{C_{inv}} = \mathrm{c}^{\mathrm{G}}_{\mathrm{inv}} \sum_{j \in \mathrm{N_G}} \mathrm{x}_j \mathrm{P}^{\mathrm{G}}_{j} + \mathrm{c}^{\mathrm{FC}}_{\mathrm{inv}} \sum_{j \in \mathrm{N_{H2}}} \mathrm{P}^{\mathrm{FC}}_{j} + \mathrm{c}^{\mathrm{EL}}_{\mathrm{inv}} \sum_{j \in \mathrm{N_{H2}}} \mathrm{P}^{\mathrm{EL}}_{j} \tag{17}$$

$$\mathrm{C_{OM}} = \sum_{t=1}^{\mathrm{N_{years}}} \frac{1}{(1+\mathrm{r})^t} \cdot \left(\mathrm{c}^{\mathrm{G}}_{\mathrm{OM}} \sum_{j \in \mathrm{N_G}} \mathrm{x}_j \mathrm{P}^{\mathrm{G}}_{j} + \mathrm{c}^{\mathrm{FC}}_{\mathrm{OM}} \sum_{j \in \mathrm{N_{H2}}} \mathrm{P}^{\mathrm{FC}}_{j} + \mathrm{c}^{\mathrm{EL}}_{\mathrm{OM}} \sum_{j \in \mathrm{N_{H2}}} \mathrm{P}^{\mathrm{EL}}_{j} \right) \tag{18}$$

$$\mathrm{C}_{sw} = \mathrm{C_{EG},}_{sw} + \mathrm{C_{Diesel},}_{sw} + \mathrm{C}^{\mathrm{L}}_{\mathrm{curl},sw} \tag{19}$$

$$\mathrm{C_{EG},}_{sw} = \mathrm{c_{EG}} \cdot \mathrm{p}^{\mathrm{G}}_{0sw} \cdot \mathrm{b}_{sw} + 0.7 \cdot \mathrm{c_{EG}} \cdot \mathrm{p}^{\mathrm{G}}_{0sw} \cdot (1 - \mathrm{b}_{sw}) \tag{20}$$

$$\mathrm{C_{Diesel},}_{sw} = \mathrm{c_{Diesel}} \sum_{k \in \mathrm{N_{Diesel}}} \mathrm{p}^{\mathrm{G}}_{ksw} \tag{21}$$

$$\mathrm{C}^{\mathrm{L}}_{\mathrm{curl},sw} = \mathrm{c}^{\mathrm{L}}_{\mathrm{curl}} \sum_{j \in \mathrm{N_L}} (1 - \mathrm{x}^{\mathrm{L}}_{jsw}) \mathrm{P}^{\mathrm{L}}_{js} \tag{22}$$

$$\mathrm{P}^{\mathrm{G}}_{0sw} \leq \mathrm{P^{EG}} \cdot \mathrm{b} \tag{23a}$$

$$\mathrm{P}^{\mathrm{G}}_{0sw} > -\mathrm{P^{EG}} \cdot (1 - \mathrm{b}) \tag{23b}$$

$$\mathrm{l}_{ijsw} \leq \overline{\mathrm{l}_{ij}} \quad \forall (i,j) \in \mathrm{E} \tag{24}$$

$$\underline{\mathrm{v}} \leq \mathrm{v}_{jsw} \leq \overline{\mathrm{v}} \tag{25}$$

$$\mathrm{H}^{+}_{2,jsw} = \alpha_{\mathrm{EL}} \cdot \mathrm{p}^{\mathrm{EL}}_{jsw} \tag{26}$$

$$\mathrm{H}^{-}_{2,jsw} = \left(\alpha_{\mathrm{FC}} \cdot \mathrm{P}^{\mathrm{FC}}_{j} + \beta_{\mathrm{FC}} \cdot \mathrm{p}^{\mathrm{FC}}_{jsw} \right) \cdot \mathrm{x}^{\mathrm{FC}}_{jsw} \tag{27}$$

$$\sum_{w \in \mathrm{W}} \sum_{s \in \mathrm{S}} \mathrm{p}_{sw} \cdot \mathrm{H}^{+}_{2,jsw} = \sum_{w \in \mathrm{W}} \sum_{s \in \mathrm{S}} \mathrm{p}_{sw} \cdot \mathrm{H}^{-}_{2,jsw} \tag{28}$$

$$\mathrm{P}^{\mathrm{G}}_{\min} \leq \mathrm{P}^{\mathrm{G}}_{j} \leq \mathrm{P}^{\mathrm{G}}_{\max} \quad \forall j \in \mathrm{N_G} \tag{29a}$$

$$0 \leq \mathrm{P}^{\mathrm{EL}}_{j} \leq \mathrm{P}^{\mathrm{EL}}_{\max} \quad \forall j \in \mathrm{N_{H_2}} \tag{29b}$$

$$0 \leq \mathrm{P}^{\mathrm{FC}}_{j} \leq \mathrm{P}^{\mathrm{FC}}_{\max} \quad \forall j \in \mathrm{N_{H_2}} \tag{29c}$$

$$0 \leq \mathrm{p}^{\mathrm{FC}}_{jsw} \leq \mathrm{P}^{\mathrm{FC}}_{j} \mathrm{x}^{\mathrm{G}}_{jsw} \tag{30a}$$

$$0 \leq \mathrm{p}^{\mathrm{EL}}_{jsw} \leq \mathrm{P}^{\mathrm{EL}}_{j} \tag{30b}$$

$$-\mathrm{P^{EG}} \cdot \mathrm{a_{w0}} \leq \mathrm{p}^{\mathrm{G}}_{0sw} \leq \mathrm{P^{EG}} \cdot \mathrm{a_{w0}} \tag{31a}$$

$$0 \leq \mathrm{p}^{\mathrm{G}}_{1\mathrm{sw}} \leq \mathrm{P^{G1}} \cdot \mathrm{a_{w1}} \tag{31b}$$

$$0 \leq \mathrm{p}^{\mathrm{G}}_{2sw} \leq \mathrm{P^{G2}} \tag{31c}$$

$$0 \leq \mathrm{p}^{\mathrm{G}}_{3sw} \leq \mathrm{P^{G3}} \cdot \mathrm{a_{w2}} \tag{31d}$$

$$0 \leq \mathrm{p}^{\mathrm{G}}_{4sw} \leq \mathrm{P^{G4}} \tag{31e}$$

$$0 \leq \mathrm{p}^{\mathrm{G}}_{5sw} \leq \mathrm{P^{G5}} \cdot \mathrm{a_{w3}} \tag{31f}$$

$$\mathrm{p}^{\mathrm{G}}_{jsw} = \mathrm{q}^{\mathrm{G}}_{jsw} = 0 \quad \forall j \in \mathrm{N} \setminus (\mathrm{N_G} \cap \mathrm{N_{slack}}) \tag{32}$$

$$\mathrm{x}^{\mathrm{L}}_{jsw} = 1 \quad \forall j \in \mathrm{N} \setminus \mathrm{N_L} \tag{33}$$

$$\mathrm{x}^{\mathrm{G}}_{jsw}, \mathrm{w}^{\mathrm{G}}_{jsw}, \mathrm{x}^{\mathrm{G}}_{j} \in \{0,1\} \quad \forall j \in \mathrm{N_G} \tag{34a}$$

$$\mathrm{x}^{\mathrm{L}}_{jsw} \in \{0,1\} \quad \forall j \in \mathrm{N_L} \tag{34b}$$

$$\mathrm{x}^{\mathrm{FC}}_{jsw} \in \{0,1\} \quad \forall j \in \mathrm{N_{H_2}} \tag{34c}$$

$$\underline{\mathrm{A}} = \begin{bmatrix} 1 & 1 & 1 & 1 \\ 0 & 1 & 1 & 1 \\ 0 & 0 & 1 & 1 \\ 0 & 1 & 0 & 1 \\ 0 & 1 & 1 & 0 \end{bmatrix} \tag{35}$$

Finally, Table I outlines the sizing limits for PV and electrolyzers, voltage constraints, and generator capacities.

TABLE I: Limits of decision variables and generator capacities

Variable	Limit
$\mathrm{P^G_{min}}$, $\mathrm{P^G_{max}}$[kW]	200, 4000
$\mathrm{P^{EL}_{max}}$, $\mathrm{P^{FC}_{max}}$ [kW]	2000
$\underline{\mathrm{v}}$, $\overline{\mathrm{v}}$ [pu]	0.81, 1.21
$\mathrm{P^{EG}}$, $\mathrm{P^{G1}}$ [kW]	4300, 1250
$\mathrm{P^{G2}}$, $\mathrm{P^{G3}}$ [kW]	1000
$\mathrm{P^{G4}}$, $\mathrm{P^{G5}}$ [kW]	600

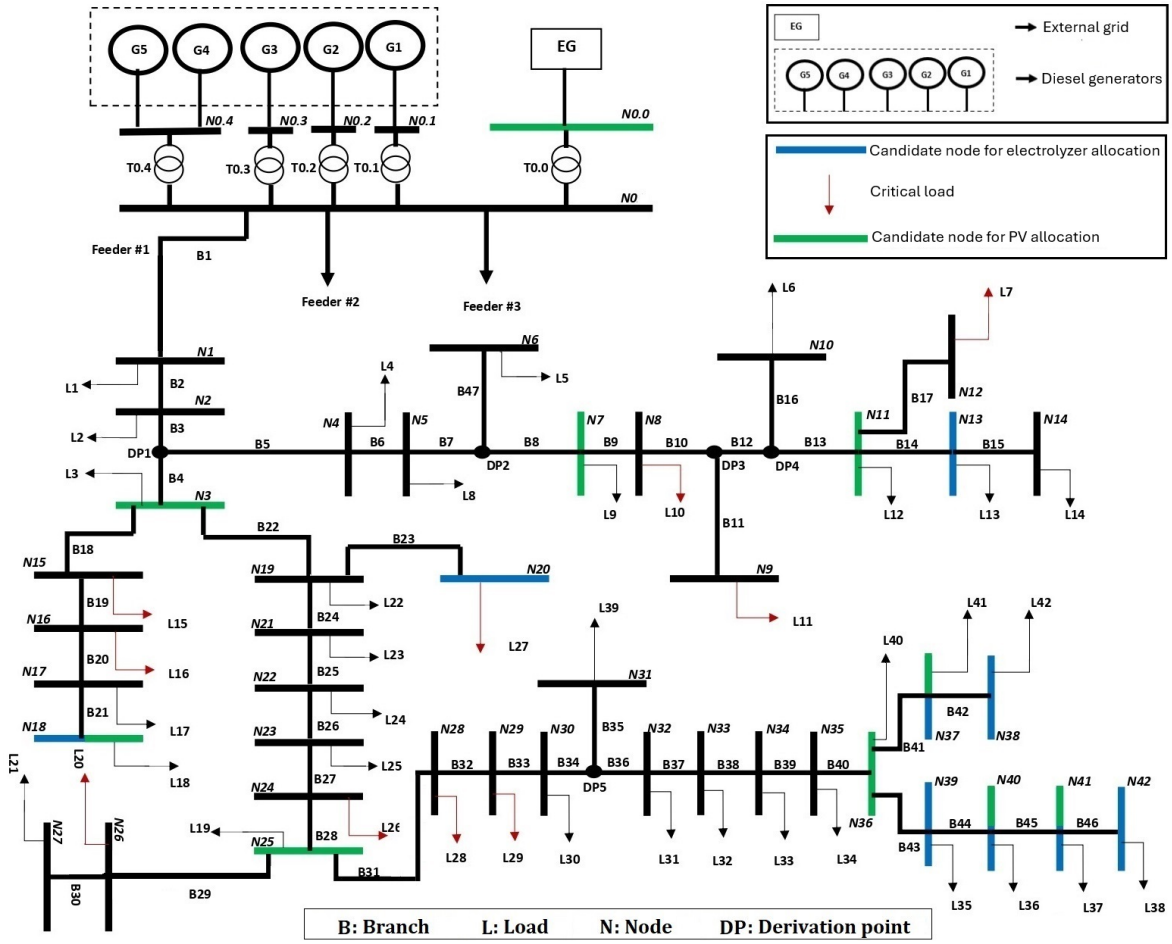

Fig. 1: Power grid of Puerto Carreño.

V. Case Study

This case study focuses on a real distribution grid in Puerto Carreño, a remote city in Colombia near the Venezuelan border. The city's connection to the external grid is weak due to its significant distance from Venezuela and ongoing political issues. The grid's transformers are often operating close to their capacity limits, and the backup Diesel Generators (DGs) are insufficient to meet peak demand during contingencies. These challenges highlight the vulnerabilities of the power system. As depicted in Fig. 1, Puerto Carreño's power grid comprises three feeders at the 13.2kV medium voltage level, dividing the grid into smaller subsystems. While Feeder #1 is detailed comprehensively, Feeders #2 and #3 are represented as significant loads. These feeders converge to the main bus N0, which is connected to the external grid N0.0 and five DGs ($\mathrm{N0.1} - \mathrm{N0.4}$). The grid supports 44 loads across 50 buses. This study leverages load time series from March and July 2019, representing sunny and rainy seasons respectively, with data sourced from [22]. Each month includes 744 hourly steps, extended across corresponding seasons to form an annual load series, merged with solar irradiance and temperature data to develop a high-dimensional probability distribution without a reactive load component (as referenced in Section II). From this, 20 representative samples are extracted for optimization, detailed in Section IV. Fig. 2 illustrates a segment of this distribution, focusing on temperature and solar radiation, and incorporates these 20 representative scenarios with their occurrence probabilities. Fig. 3 shows the distribution of ϵ^{PV}, highlighting lower solar radiation probabilities at night and a wider spread of positive values in daylight, demonstrating the influence of solar altitude and cloud cover on solar energy availability.

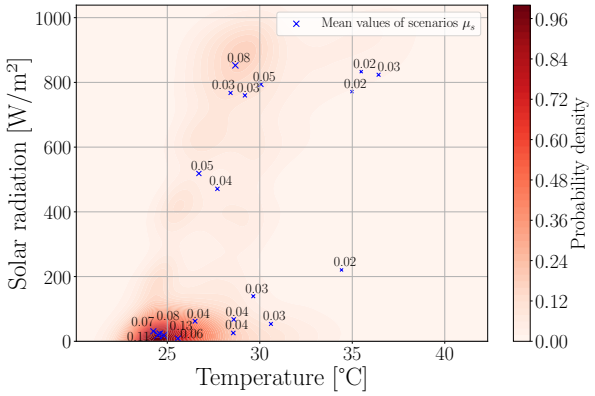

Fig. 2: Temperature and Solar Radiation Distribution.

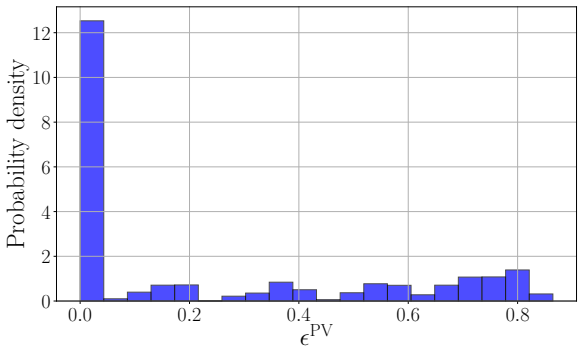

Fig. 3: Probability Distribution of total PV System Efficiency including weather conditions.

A. Contingency Scenarios

The study considers three distinct contingency scenarios:

1) Scenario 1: Normal Operation Mode: Both the external grid and all DGs are active and interconnected.

2) Scenario 2: External Grid Omission (N-1 criteria): While the external grid is disconnected, all DGs remain operational. Historical data determines the probability of an external grid contingency. On average, outages last about $84\mathrm{h}$ each month, which translates to a 11.29% downtime.

3) Scenario 3: External Grid and Single Diesel Generator Omission (N-2 criteria): This scenario contemplates a situation where there is an external grid failure, and concurrently, a DG is undergoing maintenance (labeled as G1-G5 in Fig. 1). Each DG undergoes maintenance for one week every six months, resulting in a maintenance probability of 3.84%. It is worth noting that generators G2 and G3, as well as G4 and G5, have the same capacity. Including all five potential outages would expand the optimization problem excessively. Therefore, only generators G1, G3, and G5 are considered for outages, with G3 and G5 having a doubled outage probability. The cumulative probability of an external grid failure occurring simultaneously with a DG maintenance is 0.434%. Despite the low likelihood of this contingency distribution-scenario, the operational DGs would be insufficient to meet demand, leading to expensive load curtailments. The costs associated with investment and O&M for each technology are detailed in Table II. Additional cost data can be found in Table III. Comprehensive technical parameters for every component are provided in Table IV. Given the significant water requirements of electrolyzers, certain nodes illustrated in Fig. 1 have been identified as potential candidate nodes for hydrogen components due to their closeness to water sources such as rivers or flood zones. Additionally, ten loads are designated as critical, meaning load curtailment is not possible for them. A summary of these candidate nodes are provided in Table V. To verify the correctness of the methodology and to evaluate the benefits of integrating PVs with hydrogen, three different configurations were examined:

1) No components installed.
2) Installation of PVs only.
3) Installation of PVs, electrolyzers and fuel cells.

TABLE II: Investment, Operative (O) and Maintenance cost [18], [23]

Component	Investment cost	O & M
PV system [$/kW]	1002	22.5
Fuel Cell [$/kW]	3000	97.5
Electrolyzer [$/kW]	2000	132.0

TABLE III: Additional cost information [22], [24]

Description	Cost
Diesel Fuel [$/kWh]	0.37
Load Curtailment [$/kWh]	3.30
Energy from External Grid [$/kWh]	0.19

TABLE IV: Technical parameters [17], [18], [19]

Component	Factor	Value
PV system	NOCT[°C]	45
PV system	$\eta^{\mathrm{PV}}_{\mathrm{conv}}$	0.95
PV system	$\mathrm{p}_{\mathrm{coef}}[10^{-3}/^{o}C]$	-3.5
Electrolyzer	η_{EL}	0.76
Electrolyzer	$\zeta_{\mathrm{H_2}}[\mathrm{kWh/kg}]$	40.27
Fuel Cells	$\alpha_{\mathrm{FC}}[\mathrm{kg/kWh}]$	0.004
Fuel Cells	$\beta_{\mathrm{FC}}[\mathrm{kg/kWh}]$	0.050
DGs (All)	Consumption [L/kWh]	0.17

TABLE V: Nodes for critical loads and candidates for electrolyzer allocation

Candidate Node	Information
N13, N18	Close to a small river
N20	Close to a flood zone
N37, N38, N39, N40, N41 And N42	Close to a big river
L7, L10, L11, L15, L16, L20, L26, L27, L28, L29	Critical loads
N0, N3, N7, N11, N18, N37, N25, N36, N40, N41	Generator nodes

VI. Results and Discussions

Figure 4 illustrates the costs associated with each of the three configurations, encompassing both the investment cost and the O&M costs for the whole power system over a 20-year period. Notably, the absence of both PVs and hydrogen devices results in the highest expenses: $11.01\mathrm{M\$}$ for load curtailment, $112.06\mathrm{M\$}$ for external grid power, and $33.66\mathrm{M\$}$ for diesel fuel consumption.

In contrast the second configuration slashes costs significantly: $3.35\mathrm{M\$}$ for load curtailment, $57.05\mathrm{M\$}$ for external grid power, and $17.28\mathrm{M\$}$ for diesel fuel consumption. This underscores the competitive advantage of PV installation, attributed to its low investment and O&M costs, leading to not only cost savings but also a reduction in CO2 emissions. Incorporating both PVs and hydrogen components into the system achieves the most cost-effective outcome. The expenses for load curtailment, external grid power, and diesel fuel consumption were reduced to $0.12\mathrm{M\$}$, $56.76\mathrm{M\$}$, and $15.05\mathrm{M\$}$, respectively.

It is important to highlight that the proposed planning methodology offers benefits extending beyond just cost reduction. Even though the optimization does not account for hydrogen infrastructure such as hydrogen tanks or networks, which may potentially lead to unforeseen additional costs, the integration of electrolyzers and fuel cells still shows significant advantages. For example, while a PV-only configuration deliv-

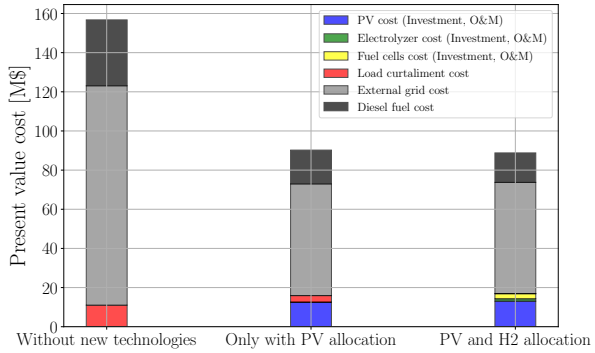

Fig. 4: Various costs of the three configurations.

ers respectable cost-related outcomes, incorporating hydrogen components enables a more extensive penetration of renewable energy sources. Furthermore, integrating PVs with hydrogen components enhances the resilience of the weak distribution grid, diminishing load curtailments. This improvement is clearly demonstrated by the reduced load curtailment costs shown in Fig. 5. The figure illustrates the third contingency scenario, depicting the simultaneous outage of an external grid and one diesel generator across different configurations.

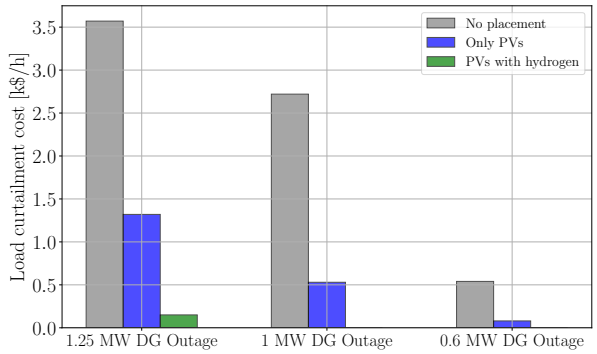

Fig. 5: Load curtailment costs for different contingency cases.

The PV-hydrogen configuration consistently assures the most minimal load curtailment costs, hitting a low of 0.0M$ for outages involving diesel generators of 1MW and 0.6MW. Only in the case of the largest generator outage of 1.25MW, a minor curtailment cost of 0.15k$/h occur, marking a substantial 96% reduction compared to the no-installation configuration.

In conclusion, Table VI enumerates the locations and sizes of the PVs for both the PV-only and PV-hydrogen configurations. It is noteworthy that the planning approach, when dependent exclusively on PVs, tends to allocate larger units near the external grid. Concurrently, Table VII provides detailed information about the fuel cells and electrolyzers for the third configuration. This data underscores the strategic and distributed placement in the combined PV-hydrogen configuration, where PVs, electrolyzers, and fuel cells are not only closely positioned but also scattered throughout the power grid, enhancing the grid's resilience and efficiency.

VII. Conclusion

In the evolving landscape of power grid planning, the integration of RESs and Hydrogen Energy Systems (HESs) offers

TABLE VI: Optimal Power and placement of PVs

Node	P[kW] - Only with PV	P[kW] - PV and H_2
N0	2305	2586
N3	3601	0
N7	0	0
N11	1453	0
N18	0	2991
N37	200	1578
N25	0	0
N36	1077	0
N40	0	1638
N41	0	200

TABLE VII: Optimal Power and placement of H_2

Node	P[kW] - Electrolyzer	P[kW] - Fuel Cell
N13	0	0
N18	95	186
N20	0	0
N37	0	0
N38	162	340
N39	0	0
N40	0	0
N41	97	131
N42	0	0

a promising avenue for enhancing grid reliability, especially in weak distribution networks. Our study in Puerto Carreño, Colombia, underscores the potential of RESs and HESs integration to overcome power supply issues. By incorporating our representative scenario generation, which utilizes Gaussian Mixture Model, the high-dimensional probability distribution was represented by a small number of highly representative scenarios. This represent both, computational efficiency and representational accuracy for the solution of the planning problem. Subsequently, a novel planning methodology was introduced in which the optimal allocation problem, coupled with curtailment options, was reformulated into a MIQCP model and solved global optimal. Our findings reveal that load curtailment costs can be significantly reduced through strategic placement of PV alone and when PV is combined with elecrolyzer and fuel cell. Notably, while the combination of PV and hydrogen components yielded the lowest cost, the optimization of hydrogen storage was not addressed, indicating potential cost increase that future research should address.

Acknowledgment

This work was funded by the Deutsche Forschungsgemeinschaft (DFG, German Research Foundation) — Project Number 450980308, by the DAAD - PROCOL research cooperation project with the title "Multimodal Microgrids for Sector Coupling in Remote Grids for Sector Coupling in Remote Grids in Colombia - MISECREG". Additionally, funding was also received through the project BPIN 2021000100003 from Universidad Nacional and MINCIENCIAS "Becas de Exelencia Doctoral" program, in Colombia.

References

[1] S. F. Contreras, C. A. Cortés, and J. M. A. Myrzik, "Probabilistic multi-objective microgrid planning methodology for optimizing the ancillary services provision," *Electric Power Systems Research*, vol. 189, no. October 2019, p. 106633, 2020. [Online]. Available: https://doi.org/10.1016/j.epsr.2020.106633

[2] T. M. Blasi, T. S. P. Fernandes, A. R. Aoki, and F. H. Tabarro, "Multiperiod Optimum Power Flow for Active Distribution Networks with Provisioning of Ancillary Services," *IEEE Access*, vol. 9, pp. 110371–110395, 2021. [Online]. Available: https://doi.org/10.1109/ACCESS.2021.3101419

[3] R. S. Pinto, C. Unsihuay-Vila, and F. H. Tabarro, "Coordinated operation and expansion planning for multiple microgrids and active distribution networks under uncertainties," *Applied Energy*, vol. 297, p. 117108, 2021. [Online]. Available: https://doi.org/10.1016/j.apenergy.2021.117108

[4] S. K. Das, S. Sarkar, and A. Bhattacharya, "Optimal Allocation of PV-Based Distributed Generations and Scheduling of Battery Storage in Grid-Connected Micro-grid Using Bi-level Optimisation," *SN Computer Science*, vol. 4, no. 5, 2023. [Online]. Available: https://doi.org/10.1007/s42979-023-02003-9

[5] X. Wu, W. Zhao, X. Wang, and H. Li, "An MILP-Based Planning Model of a Photovoltaic/Diesel/Battery Stand-Alone Microgrid Considering the Reliability," *IEEE Transactions on Smart Grid*, vol. 12, no. 5, pp. 3809–3818, 2021. [Online]. Available: https://doi.org/10.1109/TSG.2021.3084935

[6] M. Borasio and S. Moret, "Deep decarbonisation of regional energy systems: A novel modelling approach and its application to the Italian energy transition," *Renewable and Sustainable Energy Reviews*, vol. 153, p. 111730, 2022. [Online]. Available: https://doi.org/10.1016/j.rser.2021.111730

[7] D. Q. Oliveira, O. R. Saavedra, K. Santos-Pereira, J. D. F. Pereira, D. S. Cosme, L. S. Veras, R. G. Bento, and V. B. Riboldi, "A critical review of energy storage technologies for microgrids," *Energy Systems*, 2021. [Online]. Available: https://doi.org/10.1007/s12667-021-00464-6

[8] M. Sterner and M. Specht, "Power-to-Gas and Power-to-X—The History and Results of Developing a New Storage Concept," *Energies*, vol. 14, no. 20, Article no. 6594, 2021. [Online]. Available: https://www.mdpi.com/1996-1073/14/20/6594. doi: 10.3390/en14206594

[9] J. Wei, Y. Zhang, J. Wang, X. Cao, and M. A. Khan, "Multi-period planning of multi-energy microgrid with multi-type uncertainties using chance constrained information gap decision method," *Applied Energy*, vol. 260, Dec. 2019, Art. no. 114188. [Online]. Available: https://doi.org/10.1016/j.apenergy.2019.114188

[10] W. Li, T. Qian, Y. Zhang, Y. Shen, C. Wu, and W. Tang, "Distributionally robust chance-constrained planning for regional integrated electricity–heat systems with data centers considering wind power uncertainty," *Applied Energy*, vol. 336, Dec. 2022, Art. no. 120787. [Online]. Available: https://doi.org/10.1016/j.apenergy.2023.120787

[11] J. Wang, P. Zeng, J. Fan, B. Jiang, and G. Ma, "Stochastic expansion planning of integrated energy system: A benders-based decomposition approach," *Energy Reports*, vol. 9, pp. 794–804, 2023. [Online]. Available: https://doi.org/10.1016/j.egyr.2023.05.215

[12] J. E. Gómez-Rocha and E. S. Hernández-Gress, "A Stochastic Programming Model for Multi-Product Aggregate Production Planning Using Valid Inequalities," *Applied Sciences (Switzerland)*, vol. 12, no. 19, 2022. [Online]. Available: https://doi.org/10.3390/app12199903

[13] D. Wei, L. Zhang, N. Zhang, J. Fang, and Q. Qian, "Optimal generation planning in a micro-grid for supplying electrical and thermal loads in order to reduce pollutant emissions," *Journal of Cleaner Production*, vol. 421, 2023, Art no. 138531. [Online]. Available: https://doi.org/10.1016/j.jclepro.2023.138531

[14] C. M. Bishop, "Pattern Recognition and Machine Learning (Information Science and Statistics)," *Springer-Verlag*, Berlin, Heidelberg, 2006, pp. 430-439, sec. 9.2. [Online]. Available: https://www.springer.com/gp/book/9780387310732

[15] X. Jin and J. Han, "K-Means Clustering," in *Encyclopedia of Machine Learning*, C. Sammut and G. I. Webb, Eds. Boston, MA: Springer US, 2010, pp. 563-564. [Online]. Available: https://doi.org/10.1007/978-0-387-30164-8_425

[16] Z. P. P. Zarina and S. Mishra, "Power oscillation reduction contribution by PV in deloaded mode," in *2016 IEEE 6th International Conference on Power Systems (ICPS)*, New Delhi, India, 2016, pp. 1-4. [Online]. Available: https://doi.org/10.1109/ICPES.2016.7584179

[17] A. Maleki and F. Pourfayaz, "Optimal sizing of autonomous hybrid photovoltaic/wind/battery power system with LPSP technology by using evolutionary algorithms," *Solar Energy*, vol. 115, pp. 471-483, 2015. [Online]. Available: https://doi.org/10.1016/j.solener.2015.03.004

[18] Y. Xie, Y. Ueda, and M. Sugiyama, "Greedy energy management strategy and sizing method for a stand-alone microgrid with hydrogen storage," *Journal of Energy Storage*, vol. 44, 2021, Art no. 103406. [Online]. Available: https://doi.org/10.1016/j.est.2021.103406

[19] Z. Huang, Z. Xie, C. Zhang, S. H. Chan, J. Milewski, Y. Xie, Y. Yang, and X. Hu, "Modeling and multi-objective optimization of a stand-alone PV-hydrogen-retired EV battery hybrid energy system," *Energy Conversion and Management*, vol. 181, 2019, pp. 80–92. [Online]. Available: https://doi.org/10.1016/j.enconman.2018.11.079

[20] M. Farivar and S. H. Low, "Branch Flow Model: Relaxations and Convexification—Part I," in IEEE Transactions on Power Systems, vol. 28, no. 3, pp. 2554-2564, Aug. 2013, doi: 10.1109/TPWRS.2013.2255317

[21] FICO Xpress Optimization, "MIP formulations and linearizations," 2017, May 15. [Online]. Available: https://msi-jp.com/xpress/learning/square/10-mipformref.pdf

[22] IPSE, "Informe telemetría mensual 2019," 2019. [Online]. Available: https://ipse.gov.co/cnm/informe-mensuales-telemetria/

[23] L. M. León, D. Romero-Quete, N. Merchán, and C. A. Cortés, "Optimal design of PV and hybrid storage based microgrids for healthcare and government facilities connected to highly intermittent utility grids," *Appl. Energy*, vol. 335, no. January, p. 120709, 2023. [Online]. Available: https://doi.org/10.1016/j.apenergy.2023.120709

[24] UPME, "Costo Incremental Operativo de Racionamiento (CRO)", 2023. [Online]. Available:https://www1.upme.gov.co/DemandayEficiencia/Paginas/costos-de-racionamiento.aspx

APPENDIX

A. Symbols

Sets:

$\mathrm{E}, \mathrm{N}, \mathrm{S}, \mathrm{W}$	Respectively, sets of connections, nodes, scenarios and contingencies
$\mathrm{N_L}, \mathrm{N_G}, \mathrm{N_{H2}}$	Sets of load curtailment candidates, generator candidate nodes, and hydrogen candidate nodes

Constants:

$\mathrm{N_{span}}, \mathrm{N_{years}}$	Number of time points in one year (8760 = 365·24), and number of years for O&M (20 years)
$\alpha_{\mathrm{FC}}, \beta_{\mathrm{FC}}$	Consumption coefficients of fuel cell (kg/kW)
α_{EL}	Production coefficient of electrolyzer (kg/kW)
ϵ_s^{PV}	Effective power coefficient of PV
$\mathrm{c_{inv}^G}, \mathrm{c_{inv}^{FC}}, \mathrm{c_{inv}^{EL}}$	Investment costs of PV, FC, and EL ($/kW)
$\mathrm{c_{OM}^G}, \mathrm{c_{OM}^{FC}}, \mathrm{c_{OM}^{EL}}$	O&M costs of PV, FC, and EL ($/kW)
$\mathrm{c_{Diesel}}, \mathrm{c_{curl}^L}$	Diesel fuel cost and load curtailment cost ($/kW)
$\mathrm{G}_s, \mathrm{T}_s$	Solar irradiance [W/m^2], and temperature [°C]
$\mathrm{r}_{ij}, \mathrm{x}_{ij}$	Resistance, and reactance of circuit ij [Ω]
$\mathrm{P_{js}^L}, \mathrm{Q_{js}^L}$	Active and reactive power load [kW, kVar]
$\eta_{\mathrm{EL}}, \zeta_{\mathrm{H2}}$	Electrolyzer conversion efficiency, and higher heating value of hydrogen.
$\underline{\mathrm{v}}, \overline{\mathrm{v}}$	Min/max voltage squared magnitude [p.u.]
$\overline{\mathrm{l}}_{ij}$	Maximum squared current through line ij [kA^2]
$\mathrm{P_{min}^G}, \mathrm{P_{max}^G}$	Minimum and maximum sizes of PV [kW]
$\mathrm{P_{max}^{EL}}, \mathrm{P_{max}^{FC}}$	Maximum sizes of EL and FC [kW]
r	Discount rate

Variables:

$\mathrm{H_{2,jsw}^+}, \mathrm{H_{2,jsw}^-}$	Hydrogen production and consumption
$\mathrm{P}_{ij}, \mathrm{Q}_{ij}, \mathrm{l}_{ij}$	Active power flow, reactive power flow, and squared current flow in ij [kW, kVar, kA^2]
$\mathrm{P_j^G}, \mathrm{P_j^{FC}}, \mathrm{P_j^{EL}}$	Sizes of PV, fuel cell, and electrolyzer [kW]
$\mathrm{p_{jsw}^{EL}}, \mathrm{p_{jsw}^{FC}}$	EL consumption and FC production [kW]
$\mathrm{p_{jsw}^G}, \mathrm{q_{jsw}^G}$	Active and reactive power of PV injected at node j at node j [kW, kVar]
$\mathrm{Q_{jsw}^G}$	Reactive power of PV [kVar]
$\mathrm{x_{jsw}^L}, \mathrm{x_{jsw}^G}$	Binary variables for load and PV curtailment
$\mathrm{x_{jsw}^{FC}}$	Binary variable for fuel cell activation
$\mathrm{w_{jsw}^G}$	Ancillary variable for PV curtailment
$\mathrm{x_j^G}$	Binary variable for PV placement
b_{jsw}	Binary variable for external grid power direction
ϵ^{PV}	Random variable for the effective power coefficient of the PV